Q. J. R. Meteorol. Soc. (1989), **115**, pp. 293–308 551.558.21:551.511.32

The effects of rotation on flow of a single layer over a ridge

By P. G. BAINES† and B. P. LEONARD‡

† *CSIRO Division of Atmospheric Research, Aspendale, Australia.*
‡ *Department of Mechanical Engineering, University of Akron, Akron, Ohio, U.S.A.*

(Received 25 February 1988; revised 18 October 1988)

SUMMARY

The effects of the Coriolis force on the hydrostatic flow of a single lower layer over a two-dimensional ridge are described. For short periods the flows resemble those of the non-rotating case, but after a few hours (in the atmospheric context) effects of rotation become significant. For steady-state flow over ridges and plateaux, critical conditions near the crest of the obstacle can control the flow in the same manner as for conventional hydraulics. However, steady disturbances are only manifested a finite distance upstream. For initial Froude number $F_o < 1$, upstream disturbances decay on the length scale $(1 - F_o^2)^{1/2}L$, where L is the Rossby deformation radius. For $F_o > 1$, upstream bores (where they exist) become arrested at a finite distance ahead of the barrier. When flow on the lee side is supercritical, steady lee-side disturbances consist of nonlinear inertial oscillations. Obstacle shape is important in determining upstream and downstream flow. The results are useful for understanding atmospheric flows over mesoscale ridges.

1. INTRODUCTION

The flow of a single layer of fluid beneath an infinitely deep homogeneous layer of lower density is a useful model for describing a number of low-level stably stratified atmospheric flow phenomena. While sophisticated numerical models are necessary for a complete description of mesoscale phenomena, simple models are often more useful for understanding the fundamental dynamics. The use of hydrostatic single-layer models to describe low-level atmospheric disturbances was initiated by Tepper (1952, 1955), who utilized the nonlinear hyperbolic equations to describe the generation and propagation of pressure jump lines. These studies were limited to short-time integrations because of the limited numerical capability of the time. Since then, single-layer (or more accurately, one-and-a-half-layer) models have been employed to describe a range of mesoscale meteorological phenomena associated with topographic effects such as coastally trapped waves (e.g. Gill 1977) and hydraulic controls of flow over mountain ranges (e.g. Baines 1980). Many of these effects are hydraulic and nonlinear in character. Recently, the evolution of non-hydrostatic phenomena such as the 'morning glory' have been studied with more elaborate models which are capable of resolving gravity current structure and the properties of undular bores (e.g. Crook and Miller 1985).

In this paper we consider the effects of rotation on the flow of a single layer over topography, where the flow is hydrostatic and two-dimensional. Studies of the character of flow over topography have ignored rotation (see Baines (1987) for a recent review), or have been essentially linear (Queney 1948; Pierrehumbert 1984), or have assumed a uniform density gradient (Pierrehumbert and Wyman 1985). For time scales of less than a few hours the effects of rotation will be small, and conventional hydraulics will apply, but for longer times rotational effects will become increasingly important and cause substantial changes to the flow. It is well known that hydraulic jumps frequently occur in one- and multi-layered models. The effects of rotation on hydraulic jump propagation have been investigated numerically by Houghton (1969), and by Parrett and Cullen (1984), the latter concentrating on numerical techniques for correctly resolving jumps. Jumps produced by flow over topography in a rotating system result in some surprising effects which do not seem to be well known, and these are the subject of this paper.

The response of a geostrophically balanced flowing stream to the introduction of topography may be regarded as a problem in geostrophic adjustment. Most studies of the response of rotating systems to imposed disturbances (reviewed by Blumen 1972) have involved linear sytems where flow is always subcritical. Whilst this is appropriate for large-scale flows, it is not necessarily so for mesoscale flows, and this paper examines adjustment in rotating systems where the fluid and wave speeds may be comparable.

We first consider situations where the obstacle is assumed to be much higher than the layer depth, so that it may be approximated by a vertical barrier. For sufficiently large times after the commencement of motion this model is not realistic because the interface at the barrier continuously rises with time, and in order to obtain steady-state solutions it is necessary to consider obstacles of finite height. In parallel with the non-rotating situation, results may be expressed in terms of two dimensionless parameters: a Froude number $F_0 = u_0/(g'd_0)^{1/2}$, where u_0 and d_0 are the initial undisturbed velocity and thickness of the layer and g' is reduced gravity. The Coriolis parameter f is important for the length and time-scales of the solution, but otherwise its value has only a relatively minor effect on the character of the solution, through the parameter $A = a/L$, where $L = (g'd_0)^{1/2}/f$ is the Rossby deformation radius and a is the obstacle half-width.

The plan of the paper is as follows. The model and equations are outlined in section 2, and numerical schemes for integrating the time-dependent equations including hydraulic jumps are described in section 3. Analytical and numerical solutions for a single layer with the obstacle modelled as a vertical barrier are described in section 4, and solutions for flow over obstacles of finite height are described in section 5. The conclusions are summarized in section 6.

2. The model and governing equations

For our investigations we utilize the following idealized model. We consider an atmosphere on an f plane, with a lower layer of constant potential temperature θ_0 and a deep upper layer of constant potential temperature $\theta_0 + \Delta\theta$, where $\Delta\theta/\theta_0 \ll 1$. The equations for hydrostatic adiabatic motion over a rigid surface are then (Tepper 1952)

$$D\mathbf{u}/Dt + f\hat{\mathbf{z}}\times\mathbf{u} = -g\Delta\theta\nabla d/\theta_0 - (1/\rho)\nabla p_0 + (1/\rho)\mathbf{F} \tag{2.1}$$

where $\mathbf{u}$, ρ and d denote the velocity, density and thickness of the lower layer respectively, f is the Coriolis frequency, p_0 is an externally imposed pressure and $\mathbf{F}$ denotes frictional forces. $\mathbf{u}$ is assumed to be independent of height z in the layer. The corresponding continuity equation is

$$\partial d/\partial t + \nabla\cdot(d\mathbf{u}) = -\int_0^d \frac{1}{\rho}\frac{D\rho}{Dt}\,dz. \tag{2.2}$$

With the equation of state for an ideal gas it may be shown that the last term in (2.2) is $O(g'd/2c_0^2)$ relative to each of the other terms, where c_0 is the speed of sound and $g' = g\Delta\theta/\theta_0$. Hence for values of d of 1 km or less this last term is small, and may be neglected. Equation (2.2) then becomes

$$\partial d/\partial t + \nabla\cdot(d\mathbf{u}) = 0. \tag{2.3}$$

If we make the assumption that $\mathbf{u}$ and d do not vary with y, the transverse coordinate, when (2.1) is integrated through the depth of the lower layer we obtain

$$\left.\begin{aligned}\frac{\partial}{\partial t}(du)+\frac{\partial}{\partial x}(du^2)-fdv&=-g'd\frac{\partial d}{\partial x}-\frac{d}{\rho}\frac{\partial p_o}{\partial x}-C_D u(u^2+v^2)^{1/2}+\frac{\partial}{\partial x}\left(\Gamma d\frac{\partial u}{\partial x}\right)\\ \frac{\partial}{\partial t}(dv)+\frac{\partial}{\partial x}(duv)+fdu&=-\frac{d}{\rho}\frac{\partial p_o}{\partial y}-C_D v(u^2+v^2)^{1/2}+\frac{\partial}{\partial x}\left(\Gamma d\frac{\partial v}{\partial x}\right)\end{aligned}\right\} \tag{2.4}$$

where now u and v denote the mean velocities in the lower layer in the x and y directions respectively, C_D is a drag coefficient for the lower boundary ($z = 0$), and Γ represents a lateral turbulent eddy viscosity. Frictional stresses at the interface have been assumed to be negligible.

We shall assume that the surface of the topography has the shape $z = h(x)$, and that the fluid velocity in the absence of topography has the constant speed U_o in both layers. The above equations may then be non-dimensionalized by taking U_o as characteristic velocity, d_o (the undisturbed layer depth) as characteristic height and $L = (g'd_o)^{1/2}/f$, the Rossby deformation radius, as characteristic horizontal length; the relevant time scale is taken to be the inertial period. Hence we define the dimensionless variables by

$$\left.\begin{aligned}&D=d/d_o, \quad \mathbf{U}=\mathbf{u}/U_o, \quad T=ft, \quad X=x/L, \quad H=h/d_o\\ &Y=y/L, \quad P_o=p_o/\{\rho(g'd_o)^{1/2}U_o\}\end{aligned}\right\} \tag{2.5}$$

and Eqs. (2.1), (2.3) in dimensionless form become, omitting the frictional terms and y dependence, and including the topography,

$$\left.\begin{aligned}\frac{\partial U}{\partial T}+F_o U\frac{\partial U}{\partial X}-V&=-\frac{1}{F_o}\frac{\partial}{\partial X}(D+H)-\frac{\partial P_o}{\partial X}\\ \frac{\partial V}{\partial T}+F_o U\frac{\partial V}{\partial X}+U&=-\frac{\partial P_o}{\partial Y}\\ \frac{\partial D}{\partial T}+F_o\frac{\partial}{\partial X}(DU)&=0\end{aligned}\right\} \tag{2.6}$$

where F_o is a Froude number defined by

$$F_o = U_o\Big/\left(g\frac{\Delta\theta}{\theta_o}d_o\right)^{1/2}. \tag{2.7}$$

With this scaling these equations are characterized by the single dimensionless parameter F_o. If the topography has a maximum height h_m we define $H_m = h_m/d_o$, and these two dimensionless parameters determine the main properties of the steady-state solution, with the obstacle shape playing a secondary role.

In the absence of topography, P_o is given by

$$U = 1 = -\partial P_o/\partial Y, \qquad V = 0 = \partial P_o/\partial X.$$

With the same scaling, Eqs. (2.4) in dimensionless form become

$$\left.\begin{aligned}
&\frac{\partial}{\partial T}(DU) + F_o \frac{\partial}{\partial X}(DU^2) - DV \\
&\quad = -\frac{1}{F_o} D \frac{\partial (D+H)}{\partial X} - D \frac{\partial P_o}{\partial X} - CU|\mathbf{U}| + \frac{1}{R_e} \frac{\partial}{\partial X}\left(D \frac{\partial U}{\partial X}\right) \\
&\frac{\partial}{\partial T}(DV) + F_o \frac{\partial}{\partial X}(DUV) + DU = -D \frac{\partial P_o}{\partial Y} - CV|U| + \frac{1}{R_e} \frac{\partial}{\partial X}\left(D \frac{\partial V}{\partial X}\right)
\end{aligned}\right\} \quad (2.8)$$

where $C = C_D U_o / f d_o$, $R_e = g' d_o / \Gamma f = F_o^{-1}(U_o L / \Gamma)$. C is therefore a (dimensionless) form of the drag coefficient and R_e is a form of Reynolds number. We have introduced two sets of equations because the inviscid set (2.6) is the more appropriate for obtaining steady-state solutions, whereas (2.8) are more appropriate for time-dependent numerical treatment; the frictional terms may be helpful for the numerical scheme, but the precise values of C and $1/R_e$ are generally not important provided that they are small.

3. Hydraulic jumps and numerical schemes

Travelling forcing effects in a one-layer (or 1½-layer) system frequently result in hydraulic jumps. These are finite amplitude disturbances in which the properties of the fluid layer change abruptly from a velocity u_u and a depth d_u to a new velocity u_d and depth d_d. They occur as a result of inherent nonlinear steepening properties of the equations. For a non-rotating system, jump speed as a function of jump amplitude may be obtained by assuming a moving steady-state structure, and employing the equations of conservation of mass and momentum. The resulting jump speed C_J relative to the upstream layer (i.e. taking $u_u = 0$) is (e.g. Long 1970)

$$C_J = (g' d_u)^{1/2} \left\{ \frac{d_d}{2 d_u} \left(1 + \frac{d_d}{d_u} \right) \right\}^{1/2}. \quad (3.1)$$

Such jumps are well known in non-rotating systems.

In geophysical rotating systems, the time taken for fluid to pass through such a jump is generally very short compared with the rotation period. Consequently, we would expect that rotation would have a negligible effect on the character of a jump *per se* (i.e. on its internal dynamics), although it would obviously affect the jump by changing the environment through which it propagates. In this way, rotation may change the properties of a jump as it propagates over a considerable distance and time.

In order to study systems containing such jumps numerically it is customary to use a scheme which can cope with jumps as a matter of course (i.e. intrinsically), rather than employing jump conditions (Eq. (3.1)) to relate the flow on each side of an existing jump. Numerical schemes must be chosen with care, as some centred differencing schemes are notoriously prone to produce artificial oscillations in the presence of discontinuities, unless unrealistically large frictional damping is employed, and the latter has its own undesirable effects. For the calculations in this paper we have utilized a third-order upwinding scheme devised by Leonard (1979). This scheme has been tested in a non-rotating system; it produces monotonic jumps of constant shape which satisfy Eq. (3.1) very closely. A slightly simpler numerical scheme which produces jumps with (apparently) some numerical oscillation but which also satisfy (3.1) has been described and tested by Parrett and Cullen (1984).

4. Disturbances with the ridge modelled as a vertical barrier

The initial effect of a steep ridge on a moving lower layer which is suddenly set into motion may be modelled by treating the ridge as a vertical barrier. We imagine that the fluid is impulsively set into motion by externally imposed pressures $P_o(X, Y, T)$, which act to accelerate the fluid rapidly to a uniform speed (unity, in dimensionless units) which is in geostrophic balance. With this taken as the initial state, Eqs. (2.6) then become

$$U_T + F_o UU_X - V = -D_X/F_o \tag{4.1}$$

$$V_T + F_o UV_X + U = 1 \tag{4.2}$$

$$D_T + F_o(DU)_X = 0 \tag{4.3}$$

with boundary conditions

$$U = 0 \quad \text{at} \quad X = 0 \tag{4.4}$$

and

$$U = D = 1, \qquad U_T = V = 0 \quad \text{at} \quad T = 0 \tag{4.5}$$

where the subscripts denote derivatives.

We may look for a solution of this system as a power series in F_o, which will be useful if F_o is small (i.e. $U_o/(g'd_o)^{1/2} \ll 1$). Writing

$$\left.\begin{aligned} U &= U_1 + F_o U_2 + F_o^2 U_3 + \ldots \\ V &= V_1 + F_o V_2 + \ldots, \qquad D = 1 + F_o D_1 + \ldots \end{aligned}\right\} \tag{4.6}$$

and substituting into (4.3) gives

$$(U_1)_{TT} + U_1 - (U_1)_{XX} = 1 \tag{4.7}$$

with the boundary and initial conditions (4.5). (U_1, V_1, D_1) is therefore the linearized solution to Eqs. (4.1)–(4.3). This system may be solved by the Laplace transform technique to give

$$U_1 = |X| \int_0^{(T^2 - X^2)^{1/2}} \frac{J_1(y)}{(y^2 + X^2)^{1/2}}\, dy \tag{4.8}$$

where J_1 is a Bessel function in the usual notation. This result may be expressed in the form

$$U_1 = \begin{cases} 1, & T < |X| \\ 1 - e^X + X \displaystyle\int_{(T^2 - X^2)^{1/2}}^{\infty} \frac{J_1(y)}{(y^2 + X^2)^{1/2}}\, dy, & T > |X| \end{cases} \tag{4.9}$$

in the region $X < 0$. Inspection of this solution shows that at $T = |X|$ we have $U_1 = 0$ for all T, so that the principal feature of the solution is a wave propagating ahead of the barrier at unit speed with a discontinuity in U_1. After the passage of this wave this solution for U_1 takes the form of a steady term which decays exponentially ahead of the barrier, on the scale of the deformation radius, together with a decaying oscillatory term.

At fixed X for T large, the integral term behaves like $(\cos T)/T^{3/2}$, so that it represents inertial oscillations which are decaying due to dispersion. From the above, corresponding expressions for V_1 and D_1 may be obtained, and these have the form

$$V_1 = \begin{cases} 0, \quad D_1 = 0, & T < |X| \\ Te^X + XT\int_{(T^2-X^2)^{1/2}}^{\infty} \dfrac{yJ_0(y)}{(y^2+X^2)^{3/2}}\,dy, & T > |X| \\ Te^X + O\left(\dfrac{\sin T}{T^{3/2}}\right), & T \gg |X| \end{cases}$$

$$D_1 = Te^X + O\left(\frac{1}{T^{3/2}}\right), \qquad T \gg |X|. \tag{4.10}$$

These show that, apart from the decaying oscillations, there is a linear increase with time in the depth and transverse geostrophic velocity of the fluid layer immediately upstream of the barrier, on the scale of the deformation radius. This build-up implies that the barrier model for the ridge is applicable only for a limited period of time, i.e. until the layer becomes higher than the barrier.

If F_0 is not small, similar behaviour is obtained. Figure 1 shows the growth of U for $F_0 = 0{\cdot}64$, and Fig. 2 shows the growth of the corresponding V field, obtained from

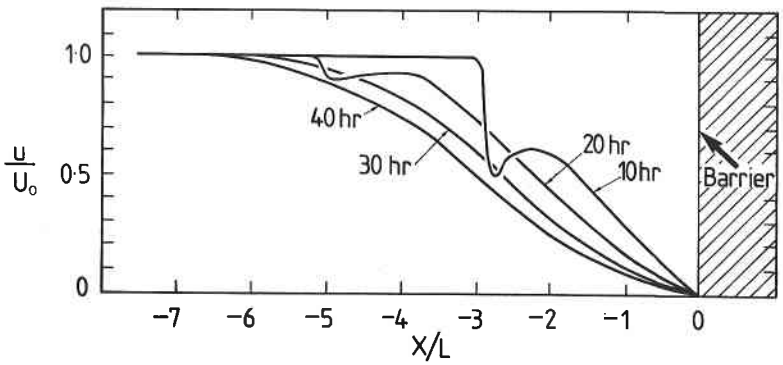

Figure 1. u field upstream of a vertical barrier at $X = 0$, with motion commencing at $T = 0$, as computed using Eqs. (2.8) with $F_0 = 0{\cdot}64$, $f = 10^{-4}\text{s}^{-1}$ (inertial period 17·45 hours), and $C_D = 0{\cdot}005$. The 40-hour curve is close to the steady state.

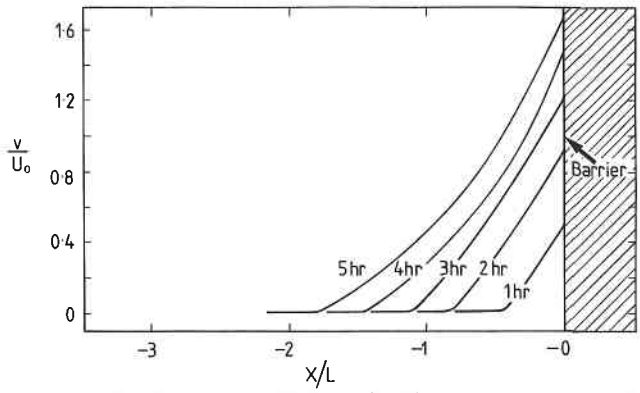

Figure 2. v component for the same conditions as for Fig. 1; v grows progressively with time.

numerical solutions to Eqs. (4.1)–(4.5) (conditions given in Fig. 1 caption). The disturbance now propagates as a hydraulic jump whose amplitude decreases monotonically with distance upstream of the barrier. The speed of this disturbance increases with increasing F_0 and jump amplitude. Also, the effect of the barrier on the U velocity does not decrease exponentially with upstream distance near the barrier, and this effect is felt somewhat further upstream than the Rossby deformation radius. Otherwise the behaviour of the flow is similar to the small F_0 case. Indeed, at $X = 0$ for all F_0 we must have (in dimensionless form)

$$U = 0, \qquad V = T, \qquad \partial D/\partial X = F_0 T$$

so that the interface must rise at a constant rate (in the mean) and the model will become invalid within the time scale of an inertial period (although the precise time will depend on F_0 and the barrier height). We therefore proceed to discuss topographic barriers of finite height, in the next section.

5. Disturbances caused by flow over ridges

If the ridge has finite height, the governing equations for the motion of the fluid surrounding it are

$$\partial U/\partial T + F_0 U \partial U/\partial X - V = -(1/F_0)\partial(D + H)/\partial X \tag{5.1}$$

together with Eqs. (4.2) and (4.3). If the relative motion of the air is initiated impulsively at time $T = 0$ in the same manner as in the previous section, the initial conditions are

$$U = 1, \qquad \partial U/\partial T = V = 0, \qquad D + H(X) = 1 \tag{5.2}$$

at $T = 0$.

(a) *Linear solutions*

For ridges which have small maximum height H_m, we may linearize these equations by writing

$$U = 1 + \hat{U}, \qquad D = 1 + \hat{D} \tag{5.3}$$

and neglecting second-order terms in $\hat{U}$, V and $\hat{D}$. Analytical solutions may then be obtained by using Laplace transforms and the method of variation of parameters (Jeffreys and Jeffreys 1962, p. 493). The steady-state solutions obtained in the large-time limit are

$$\hat{D} = -\frac{H}{1 - F_0^2} + \frac{1}{2(1 - F_0^2)^{3/2}} \left\{ \int_X^\infty \exp\left(\frac{X - \xi}{(1 - F_0^2)^{1/2}}\right) H(\xi)\, d\xi + \right.$$

$$\left. + \int_{-\infty}^X \exp\left(-\frac{(X - \xi)}{(1 - F_0^2)^{1/2}}\right) H(\xi)\, d\xi \right\}, \quad F_0 < 1 \tag{5.4}$$

$$\hat{D} = \frac{H}{F_0^2 - 1} + \frac{1}{(F_0^2 - 1)^{3/2}} \int_{-\infty}^X H(\xi) \sin\left(\frac{\xi - X}{(F_0^2 - 1)^{1/2}}\right) d\xi, \quad F_0 > 1. \tag{5.5}$$

For $F_0 < 1$ the disturbance decays exponentially upstream and downstream of the obstacle on a scale of $(1 - F_0^2)^{1/2} L$. For $F_0 > 1$ there is no upstream disturbance at all, and the downstream motion consists of inertial lee waves. For such waves of the form $e^{i(kx - \omega t)}$ in a layer at rest, the dispersion relation is

$$\omega^2 = f^2 + c^2 k^2 \tag{5.6}$$

where $c^2 = g'd_o$. The phase velocity $c_p = \omega/k$ and group velocity $c_g = \partial\omega/\partial k$ are given respectively by

$$c_p^2 = c^2 + f^2/k^2, \qquad c_g c_p = c^2 \tag{5.7}$$

so that $c_g < c < c_p$. Hence wavetrains may be stationary in a stream for supercritical flows but not for subcritical flows and, as for the case of pure gravity waves, they will occur on the downstream side of the source.

(*b*) *Numerical solutions*

To obtain time-dependent solutions for finite values of H_m, Eqs. (5.1), (5.2), (4.2) and (4.3) must be solved numerically. This has been done for various obstacle shapes for a range of values of F_o (actually the equations used were in the form of Eq. (2.4)), using the procedures described in Leonard (1979). Two basic obstacle shapes were used for the numerical studies: a symmetric obstacle with parabolic shape, and a semi-infinite plateau-shaped obstacle with a parabolic nose and flat top. Values of $A = a/L$ used ranged from 0·01 to 10, where a is the horizontal distance between zero and maximum obstacle height on the upstream side. Two representative solutions are shown in Figs. 3 and 4 for semi-infinite obstacles. Figure 3 shows the interface height at four-hour intervals for $F_o = 0{\cdot}85$ and $H_m = h_m/d_o = 2/3$. A bore propagates upstream with its amplitude and speed decreasing with time, and the interface approaches a steady shape which is approximately exponential ahead of the ridge. After 20 hours, a residual bore still exists, and the surge associated with it has almost become detached from the steady-state perturbation. At a given X, the associated V field progressively increases after the bore passes from zero to a steady value, and this steady-state profile is shown in the upper part of the figure. The steady-state flow ahead of the obstacle is qualitatively similar to that of the linear solution described above.

The results from numerical computations for $F_o = 1{\cdot}5$ and the same H_m value as in Fig. 3 are shown in Fig. 4. Again, an upstream jump moves ahead of the obstacle, but the jump amplitude decreases with time and its speed (relative to the obstacle) falls to zero. It therefore stops at a fixed distance ahead of the ridge, which in this case is reached after about 12 hours. In situations where $F_o > 1$, therefore, when a hydraulic jump forms upstream of the obstacle, the Coriolis force causes it to become stationary. This contrasts with the linear solution, which has no disturbance ahead of the obstacle at all. These numerical solutions show the general character of the steady-state solutions when H_m is not small. Numerical solutions for symmetric obstacles of finite length for the same parameter values show the same behaviour on the upstream side of the obstacle as do those for the semi-infinite obstacles, but of course the downstream details are different.

(*c*) *Nonlinear solutions*

One may use this information to obtain the general properties of these steady-state solutions over a wide range of values of F_o and H_m by semi-analytical methods. Equations (5.1), (4.2) and (4.3) in steady-state form become

$$\left.\begin{aligned} F_o U\frac{dU}{dX} - V &= -\frac{1}{F_o}\frac{d}{dX}(D+H) \\ F_o U\frac{dV}{dX} + U &= 1 \\ UD &= 1. \end{aligned}\right\} \tag{5.8}$$

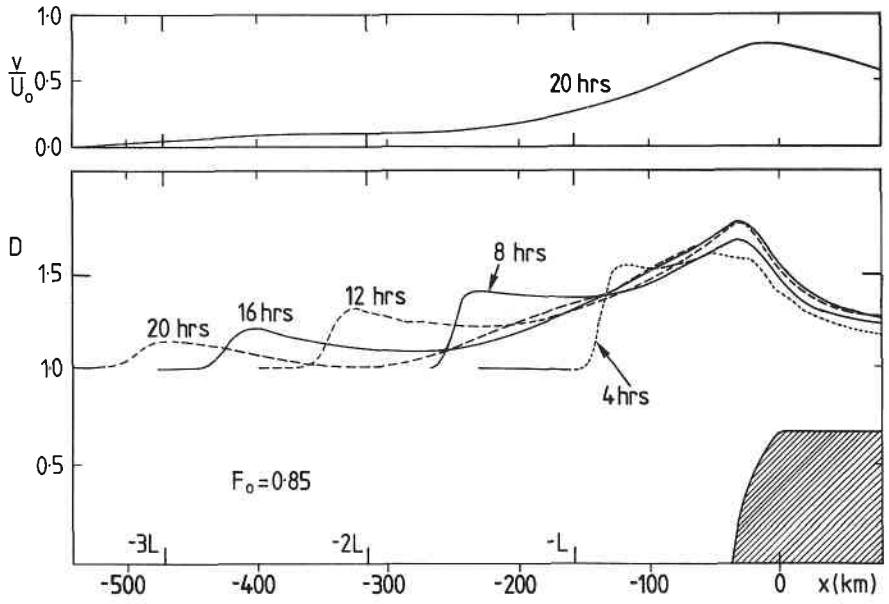

Figure 3. Growth of the disturbance with time upstream of a semi-infinite obstacle with $F_o = 0{\cdot}85$, $H_m = 0{\cdot}667$, $f = 10^{-4}s^{-1}$, $L = 157$ km, as represented by the interface height. Note the early resemblance to non-rotating flow, the subsequent decrease of the amplitude of the bore, and the detached upstream disturbance at 20 hours. The transverse velocity v at 20 hours is shown in the upper part of the figure.

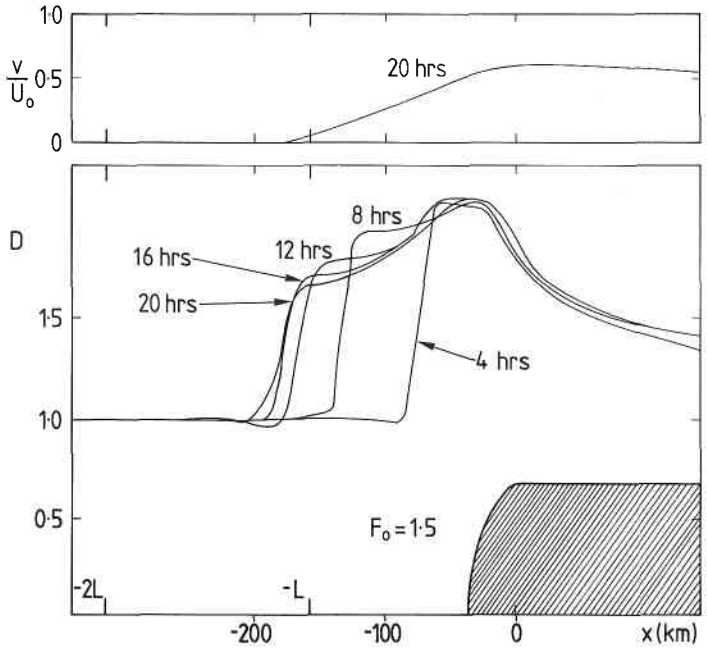

Figure 4. As Fig. 3, but with $F_o = 1{\cdot}5$.

Eliminating U then gives

$$(1 - F_o^2/D^3)dD/dX = F_o V - dH/dX \tag{5.9}$$

$$dV/dX = (D - 1)/F_o. \tag{5.10}$$

We solve these equations for a representative $H(X)$ of the form

$$H(X) = \left\{ \begin{array}{ll} 0, & X < -A \\ H_m X/A, & -A < X < 0 \\ H_m, & X > 0 \end{array} \right\} \tag{5.11}$$

representing a ramp-nosed semi-infinite obstacle, with boundary conditions

$$D \to 1, \qquad U \to 1, \qquad V \to 0 \qquad \text{as} \qquad X \to -\infty. \tag{5.12}$$

From Eq. (5.9) one can see that where $F_o V = dH/dX$ we must have

$$dD/dX = 0 \qquad \text{or} \qquad D = F_o^{2/3}. \tag{5.13}$$

The first alternative corresponds to solutions which are everywhere sub- or supercritical, and includes the linear perturbation solutions described above (Eqs. (5.4) and (5.5)). The second alternative corresponds to the same critical condition ($u = (g'd)^{1/2}$ in dimensional notation) as that for non-rotating systems; note, however, that the same physical interpretation that a wave propagating against the stream is stationary does not apply here unless the wave is short ($k \to \infty$). Further, the additional term due to the earth's rotation means that the *shape* of the obstacle (as well as H_m) can now affect the character of the solution.

We discuss the solutions of Eqs. (5.9), (5.10) for $F_o < 1$ and $F_o > 1$ in turn. Details of the procedure are given in the appendix.

$F_o < 1$: For $X < -A$ the equations may be integrated to give

$$V^2 = \frac{1}{F_o^2}\left(\frac{D-1}{D}\right)^2 (D^2 - F_o^2) \tag{5.14}$$

$$\frac{dD}{dX} = D^2(D-1)\frac{(D^2 - F_o^2)^{1/2}}{(D^3 - F_o^2)}, \qquad X < -A. \tag{5.15}$$

Integration of (5.15) gives the solution curve for D for $X < -A$, and this solution is determined by $D(-A)$, the value of D at $X = -A$. The curve very roughly resembles an exponential profile. For flows which are subcritical (i.e. $D > F_o^{2/3}$) everywhere, if the solutions are to be bounded they must satisfy the conditions

$$D \to 1, \qquad V \to 0 \qquad \text{as} \quad |X| \to \infty. \tag{5.16}$$

This implies that for $X > 0$, D must again satisfy (5.15), but with a change in sign of the right-hand side. If on the other hand $D = F_o^{2/3}$ somewhere, this critical condition 'controls' the solution. For the ramp-shaped obstacle, it occurs at the top of the ramp ($X = 0$) where dH/dX changes rapidly. Upstream of this point ($X < 0$) the character of the solution is the same as for the subcritical case, but for $X > 0$ it is different, as discussed below. The flow states are shown schematically in Figs. 5(a) and (b). The dependence of flow properties on obstacle shape, with $A = 0{\cdot}01$, $1{\cdot}0$ and $10{\cdot}0$, is shown in Figs. 6(a, b and c). Conclusions obtained for ramp-shaped obstacles were also found to hold in general for symmetrical obstacles, with the same shape on their upstream side, apart from quantitative differences in downstream flow.

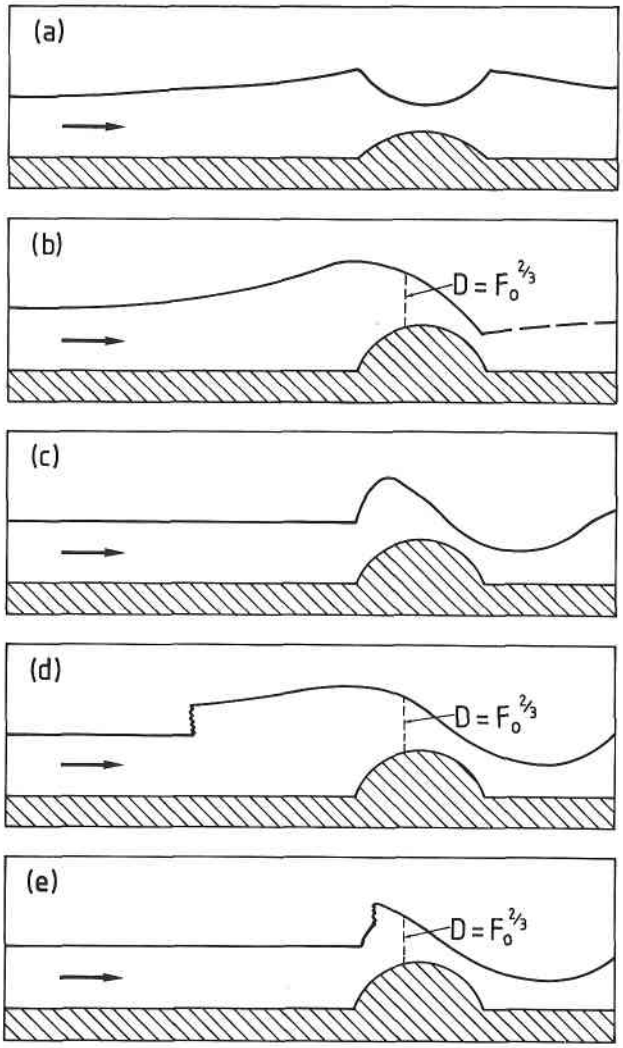

Figure 5. Schematic representations of the various possible flow configurations: (a) $F_o < 1$, $D > F_o^{2/3}$ everywhere; (b) $F_o < 1$, flow critical over obstacle; (c) $F_o > 1$, $D < F_o^{2/3}$ everywhere; (d) $F_o > 1$, flow critical over obstacle, stationary upstream jump; (e) $F_o > 1$, flow critical over obstacle, stationary jump on upstream face of obstacle.

$F_o > 1$: For the flows which are *everywhere* supercritical (i.e. $D < F_o^{2/3}$ everywhere) there is no upstream disturbance, so that $D(-A) = 1$. The flow further downstream may be found by integration, and the wake of the obstacle (or ramp) is found to consist of finite amplitude inertial waves. On the other hand, if H_m is sufficiently large for the flow to become critical somewhere ($D = F_o^{2/3}$)—at or near the obstacle crest, or at the top of the ramp—this critical condition forces an upstream jump which becomes stationary at a fixed location upstream. The various possible flow states are shown schematically in Figs. 5(c, d and e). Regions of the F_o–H_m plane where these various states are found for $A = 0{\cdot}01, 1{\cdot}0, 10{\cdot}0$ are shown in Figs. 6(a, b and c) respectively. We note that, for $F_o > 1$, there is a parameter range where the upstream jump is located over the ramp, rather than upstream of it. For these hydrostatic flows there is only one steady state for each

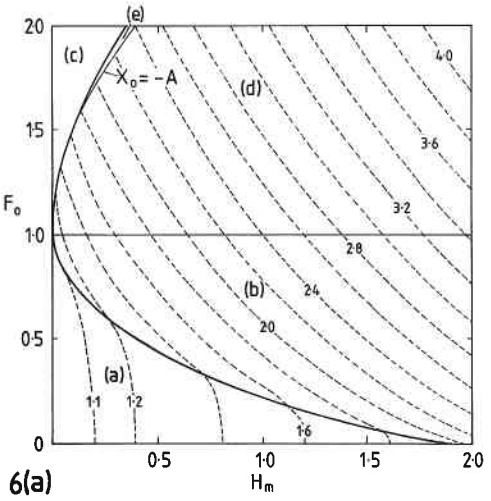

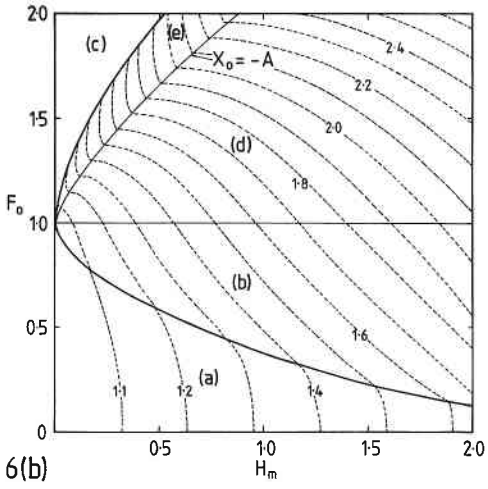

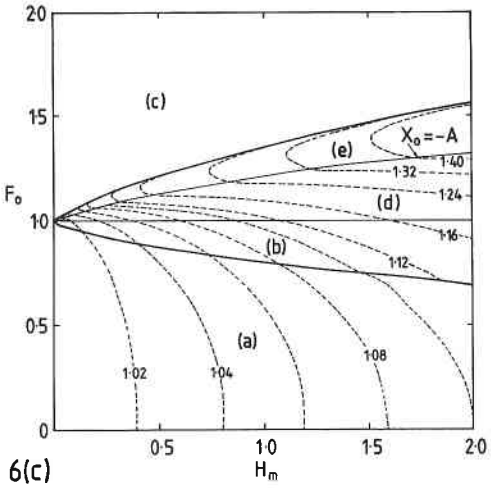

Figure 6. F_o–H_m diagrams for $A = 0{\cdot}01$ (a), $1{\cdot}0$ (b) and 10 (c). The regions marked (a), (b), (c), (d) and (e) denote the corresponding flow configurations in Fig. 5, with the boundaries of these regions marked by solid lines. Dashed lines represent constant values of $D(-A)$, except in region (e) where they represent the value of D.

set of values of F_o, H_m and A; the multiple equilibria and hysteresis phenomena found in non-rotating flows with $F_o > 1$ (Baines and Davies 1980; Baines 1987) are not present.

The nature of the flows downstream is particularly significant. As described above, if $F_o < 1$ and $D > F_o^{2/3}$ everywhere, the flow satisfies $D \to 1$, $V \to 0$ as $|X| \to \infty$. But if the flow is everywhere supercritical, or passes through a critical state ($D = F_o^{2/3}$) near the obstacle crest, then the downstream flow is mostly also supercritical with finite amplitude inertial oscillations. These oscillations are governed by

$$\left(\frac{dD}{dX}\right)^2 = \frac{D^6}{(D^3 - F_o^2)^2}\left(\frac{(D-1)^2(D^2 - F_o^2)}{D^2} - \frac{(D_o - 1)^2(D_o^2 - F_o^2)}{D_o^2}\right), \qquad (5.17)$$

where $V = 0 = dD/dX$ when $D = D_o$, and they have a maximum amplitude of $D = F_o^{2/3}$. The solutions of this two-parameter (F_o and D_o) system represent periodic waves with peaked crests and broad troughs, with D oscillating between two values of D_o. For the waves of maximum amplitude where $D_o = F_o^{2/3}$, the minimum value of D, $D_{\min}$, is given by the smaller root of

$$(D-1)^2(F_o^2/D^2 - 1) = (F_o^{2/3} - 1)^3 \qquad (5.18)$$